El Niño-Southern Oscillation Impacts on Winter Winds over Southern California

Neil Berg, Alex Hall, Scott Capps, and Mimi Hughes, Dept. of Atmospheric and Oceanic Sciences, UCLA

Abstract

Changes in wintertime 10 m winds due to the El Niño-Southern Oscillation (ENSO) are examined using a 6 km resolution climate simulation of Southern California covering the period from 1959 through 2001. Wind speed statistics based on regional averages reveal a general signal of increased mean wind speeds and wind speed variability during El Niño across the region. An opposite and nearly as strong signal of decreased wind speed variability during La Niña is also found. In spite of these regional-scale generalizations, there are significant sub-regional mesoscale structures in the wind speed impacts. In some cases, impacts on mean winds and wind variability at the sub-regional scale are opposite to those of the region as a whole. All of these signals can be interpreted in terms of shifts in occurrences of the region's main wind regimes due to the El Niño phenomenon. A hypothetical offshore wind farm is used to illustrate how the surface circulation impacts would affect wind power in the region. The results of this study can be used to understand how interannual wind power variations in regions of Southern California are influenced by the El Niño phenomenon. To the degree the phenomenon is predictable, they may also have implications for predictability of wind power on interannual time scales.

Wind dataset development

Southern California regional climate simulation

- **Model**: Penn State/NCAR mesoscale model version 5, release 3.6.0 (MM5)
- **Temporal extent**: 1 January 1959 through 31 December 2001
- **Horizontal resolution**: Three nested domains: 54 km → 18 km → 6 km
- **Vertical resolution**: 23 sigma levels in each domain
- **Boundary conditions**: ERA-40 (125 km) reanalysis dataset
- **Cumulus parameterization**: Kain-Fritsch 2 (outer two domains), explicitly resolved convection in innermost domain
- **Planetary boundary layer**: MRF scheme
- **Microphysics**: Dudhia simple ice scheme
- **Radiation**: Dudhia longwave/shortwave interactions with clear-air and cloud

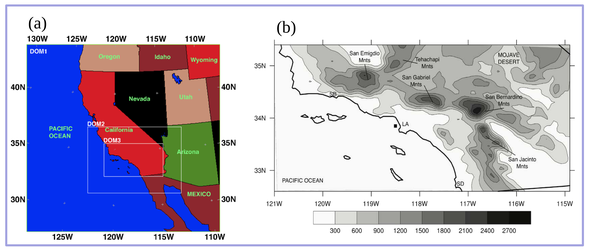

Fig. 1: *(a) Three domains of the MM5 simulation. The horizontal resolution in the outermost domain, middle, and innermost domains are 54 km, 18 km, and 6 km, respectively (Figure from Hughes et al. (2007), Clim Dyn, **29**, 277-292). (b) Innermost 6 km domain with topography contoured and hypothetical wind farm location (black square) off the Los Angeles coast.*

Winter mode classification

Winters are classified as either El Niño, La Niña, or neutral when the corresponding DJF-mean Niño 3.4 region (5˚ N-5˚ S, 120˚ -170˚ W) sea surface temperature anomaly (SSTA) is greater than or equal to +0.6˚ C, less than or equal to -0.6˚ C, and between +0.6˚ C and -0.6˚ C, respectively (Table 1). Niño 3.4 SSTA values were provided by the NOAA Climate Prediction Center (http://www.cpc.ncep.noaa.gov/data/indices/sstoi.indices).

El Niño winters	Neutral winters	La Niña winters
1964, 1966, 1969, 1970, 1973, 1983, 1987, 1988, 1992, 1995, 1998	1960, 1961, 1962, 1967, 1975, 1977, 1978, 1979, 1980, 1981, 1982, 1990, 1991, 1993, 1994, 1997	1963, 1965, 1968, 1971, 1972, 1974, 1976, 1984, 1985, 1986, 1989, 1996, 1999, 2000, 2001

Table 1: *The classification of winters based on the DJF-mean Niño 3.4 sea surface temperature anomaly. The year of each winter is composed of December of the previous year and January and February of the current year, e.g. 1992 includes December 1991, January and February 1992.*

10 m wind processing

A 42 winter-long time series (Dec. 1959 - Feb. 1960 through Dec. 2000 – Feb. 2001) of daily-mean 10 m wind component and speed anomalies was created by:

1. Calculating daily-mean 10 m wind components and speeds from hourly values
   - this step removes influences of local diurnal circulations (land/sea breeze, diurnal mountain winds)
2. Calculating daily-climatological components and speeds
   - each day in our simulation occurs 42 times, so daily-climatological values are found by averaging all 42 daily-mean wind components and speeds
3. Subtracting daily-climatologies from daily-means to produce daily-mean anomalies

Regional and local analyses

We examine both regional and local ENSO impacts to the mean and standard deviation of daily-mean 10 m wind component and speed anomalies.

• Regional-scale impacts are quantified by averaging wind anomalies across the domain before computing the mean and standard deviation of daily-mean anomalies for each winter. This provides a region-wide perspective on ENSO impacts.
• To quantify local impacts, we first produce aggregated El Niño, La Niña, and neutral time series of daily-mean anomalies (see Table 1). The mean and standard deviation of each aggregated time series at each grid point is then computed. This yields three (El Niño, La Niña, and neutral) means and standard deviations per grid point. A comparison of these phase-based means and standard deviations provides a local perspective on ENSO impacts.

Contact: nberg@atmos.ucla.edu

ENSO impacts on the mean and standard deviation of 10 m winds

ENSO teleconnection dynamics

ENSO influences the Northern Hemisphere subtropical jet stream and storm tracks as Rossby waves propagate out of anomalously warm, convective regions in the Pacific Ocean and across North America. The jet stream extends eastward and equatorward during El Niño. Storm tracks also extend eastward toward the West Coast of North America. During La Niña, the jet recedes toward the west and also shifts poleward, while the storm tracks also shift poleward into the Gulf of Alaska (e.g. Straus and Shukla (1997), *J Atmos Sci*, **54**, 777-790). During El Niño, the southern US regions align with a stronger and more direct jet stream and experience a higher frequency of passing storms. During La Niña, these regions coincide with a weaker and less direct jet stream and experience fewer storms. Southern California is hypothesized then to have higher average and more variable wind speeds during El Niño, with the opposite effect during La Niña.

Regional-scale impacts

Time series of the mean and standard deviation of domain-averaged 10 m wind speed anomalies are presented in Figure 2. A signal of ***increased variability during El Niño events*** is evident in the standard deviation time series. Four of the five highest standard deviations (1983, 1969, 1998, 1988) happen during El Niño winters. Amongst the five lowest standard deviations, none are found during El Niño. An opposite signal of ***decreased variability is also found for the La Niña phase***. Four of the five lowest standard deviations are recorded during La Niña winters (1976, 1968, 1986, 1996). None of the five highest standard deviations occur during La Niña.

Fig. 2 also reveals that ***higher wind variability is generally accompanied by higher mean winds, and vice versa***. There is a significant positive correlation (r = 0.46, p = 0.002) between the mean and standard deviation time series. This relationship may be orchestrated in part by the ENSO phenomenon. Four of the top five (1998, 1973, 1969, 1964) and half of the ten highest means are during El Niño winters. Two of five lowest means also occur during El Niño winters (1995, 1970). However, unlike the variability case where an opposite La Niña signal is found, no clear La Niña signal is seen in the time series of the means.

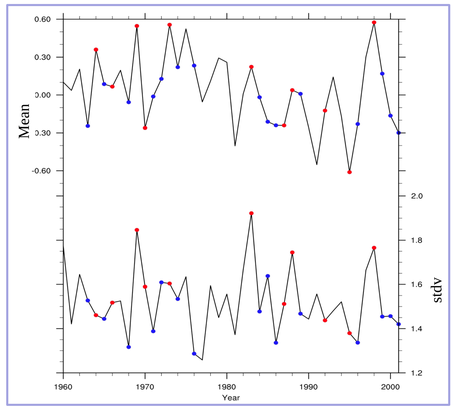

Fig. 2: *Time series showing the mean and standard deviation of the domain-averaged, 10-m daily-mean wind speed anomalies. Red dots indicate El Niño winters and blue dots indicate La Niña winters. Unit for each time series is m s^{-1}.*

Local-scale impacts

Figure 3 shows maps of the average differences in the mean and standard deviation of the daily-mean 10 m wind speed anomalies between the ENSO phases. During El Niño, 78% of the domain typically experiences increased wind speed variability (Fig. 3c). This is greater than the portion of the domain that experiences increased precipitation variability during El Niño (64%, not shown). During La Niña, a majority of the domain (66%) experiences decreased variability (Fig. 3d). Higher average wind speeds are typically experienced over 65% of the domain during El Niño (Fig. 3a). Meanwhile, 79% of the domain experiences lower average speeds during La Niña (Fig. 3b).

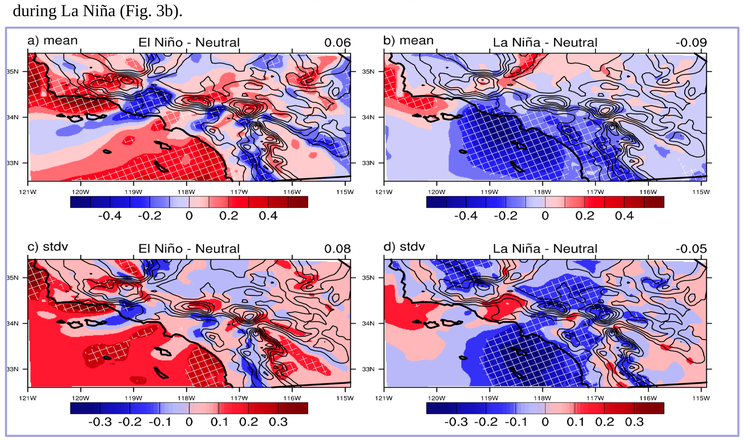

Fig. 3: *Average differences of the mean and standard deviation (stdv) for daily-mean 10 m wind speed anomalies between El Niño (a,c) and La Niña (b,d) winters compared to neutral winters. Contour interval is 0.1. Positive differences are shaded red and negative differences are shaded blue. Regions with significant differences (at the 90% level using the t-test) are hatched. The domain-averaged value is reported on the top right of each plot. Unit for each plot is m s^{-1}.*

Understanding spatial structures and relation to large-scale circulation

The spatial structures of Fig. 3 may be understood by examining changes in the main wintertime wind regimes of Southern California, which are classified using a cluster analysis technique (details in Conil and Hall (2006), *J Clim*, **19**, 4308-4325). The first step in the cluster analysis is to perform a real vector empirical orthogonal function (EOF) analysis on the 42-winter time series of daily-mean 10 m wind speed anomalies. The first EOF accounts for nearly 45% of the variance and the second for nearly 36%. Also included in the EOF analysis is a corresponding time series of daily amplitudes (i.e. principal components) associated with the first two EOFs (PC1 and PC2). These daily PC values are depicted as a scatter plot in PC-space in Figure 4. A cluster analysis is then performed on the PC time series to classify daily wind patterns into three main wintertime wind regimes. Using this method, 92% of all daily wind fields can be classified into one of three prominent wintertime wind regimes: northwesterly, Santa Ana, and onshore. By averaging daily winds within each cluster, composite wind fields (Fig. 5) are produced to reveal the spatial patterns of each wintertime wind regime. We also find the average occurrence of each principal wind regime according to ENSO phase, which is shown in Table 2. The spatial structures of both El Niño and La Niña impacts (Fig. 3) can be understood by examining Figs. 3 and 5 and Table 2.

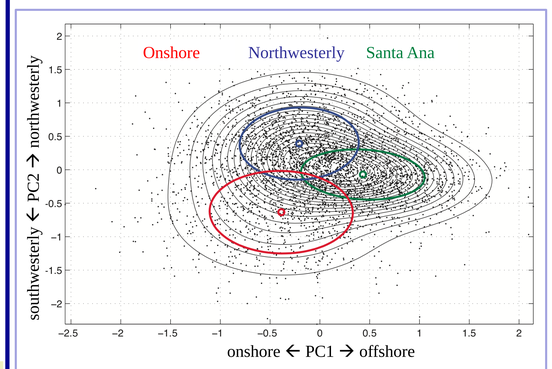

Figure 4: *Scatter plot of the leading two principal components (PC1, PC2) for each day in the 42-winter time series (black dots). The cluster model provides a PDF estimate of the data distribution (black contours). Clustered wind patterns are defined by covariance ellipses with semi axes of two standard deviations (dark lines) from the cluster means (open circles).*

	Santa Ana	Northwesterly	Onshore
El Niño	31	33	18
Neutral	37	32	15
La Niña	35	37	13

Table 2:*Average occurrence of each principal wind regime (days per winter) according to ENSO phase*

El Niño spatial structures

The spatial structures of the El Niño impacts (Fig. 3a,c) can be explained by examining Table 2 and Fig. 5. As seen in Table 2, the ***onshore regime occurs more frequently than usual during El Niño***, reflecting the southward displaced jet stream in this phase. Frequent southward incursions of the jet stream bring greater average winds through the Southern California Bight. However, the southward displacement of the jet stream is not constant and the intermittent reappearance of the other two regimes results in enhanced wind speed variability throughout the Bight. Referring to composite wind fields in Fig. 5, calm conditions over major mountain complexes associated with the northwesterly regime tend to be replaced by stronger average winds as the onshore regime becomes more frequently established. The resulting more frequent alternation between calm and strong winds also leads to greater wind speed variability over the mountain complexes. Effects on both mean and variability are enhanced as elevation increases, since the onshore flows are forced to accelerate as they ascend and their vertical extent decreases. Lower average wind speeds within the major mountain passes reflect ***decreased Santa Ana events during El Niño*** (Table 2); strong winds associated with the Santa Ana regime in these areas become replaced by calmer conditions of the more frequently established onshore regime.

La Niña spatial structures

The results in Table 2 also help to explain the spatial structures of the La Niña impacts (Fig. 3b,d). ***During La Niña conditions, the northwesterly regime occurs more frequently than usual at the expense of the onshore regime.*** This leads to slightly greater winds over the western half of the Southern California Bight and significantly weaker winds over the eastern half of the Bight and coastal basin, as seen in Fig. 5. Since the onshore regime occurs less frequently during La Niña, lower variability is found in much of the Southern California Bight and over the mountain complexes, i.e. the regions that correspond to higher variability during El Niño (Fig. 3a,c). Greater variability along prominent mountain passes during La Niña is also tied to a reduction of onshore events. Winds in the passes are very weak during an onshore event. With fewer onshore events during La Niña, alternations between strong winds of the Santa Ana regime and the weak winds of the northwesterly regime become more frequent. This vacillation likely leads to increased wind speed variability in the passes.

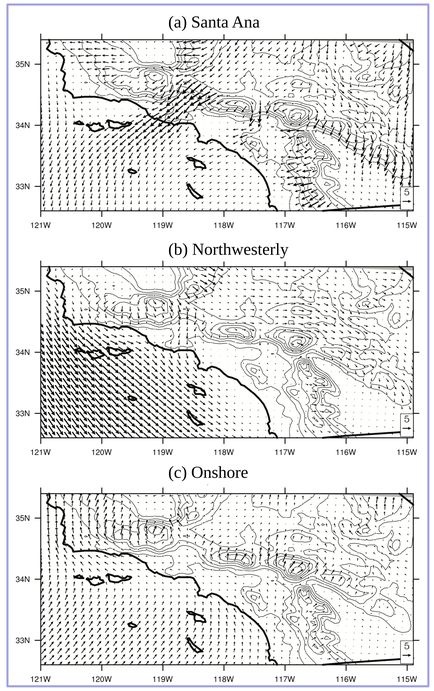

Fig. 5: *10 m wind composite maps corresponding to the three clustered wind regimes produced by the mixture model. The reference vector has a magnitude of 5 m s^{-1}.*

Wind power impacts

To illustrate how the ENSO impacts on surface circulation in Southern California would affect wind power, we examine our results from the prospective of a hypothetical wind farm. The proposed 6 km by 6 km wind farm is located at 33.8˚ N and 118.5˚ W (see Fig. 1). If the rotor diameter of the turbine is 77 m, this area could hold approximately 200 turbines, determined by using a 4 diameter by 7 diameter turbine spacing. This location is selected for its proximity to the large LA metropolitan area and because of the large ENSO impacts there (Fig. 3). Bathymetric data needed for offshore turbine foundation planning and an exclusionary factor that represents the fraction of potential unusable waters in the region are neglected in this hypothetical calculation.

We first used a cubic spline approach to vertically interpolate hourly zonal and meridional wind components to a typical hub-height of 80 m above the ground using the simulation's wind components at the eight lowest half-vertical levels (from approximately 38 to 1,890 m). This interpolation was based on the same boundary layer scheme used in the simulation- the MRF boundary layer scheme. Hourly 80 m wind speeds at each grid point were translated into wind power using the power curve of the GE 1.5sle MW wind turbine (http://www.gepower.com/prod_serv/products/wind_turbines/en/15mw/specs.htm). For speeds less than the cut-in speed (3 m s^{-1}) or greater than the cut-out speed (25 m s^{-1}), the power output was specified to be zero. Winds at 14 m s^{-1}, the rated speed, produce the maximum wind power of 1.5 MW.

The average hourly wind power output during El Niño, La Niña, and neutral winters for the hypothetical wind farm was found to be ~71, 56, and 65 MW, respectively. Compared to neutral conditions, this translates to an ***increase of wind power output at the proposed farm by approximately 9% during El Niño and a decrease of approximately 14% during La Niña***. The standard deviation of hourly wind power across the wind farm during El Niño, La Niña, and neutral winters was found to be ~101, 90, and 97 MW, respectively. Compared to neutral winters, this translates to ***increased wind resource volatility by 4% during El Niño and decreased volatility by 7% during La Niña.***

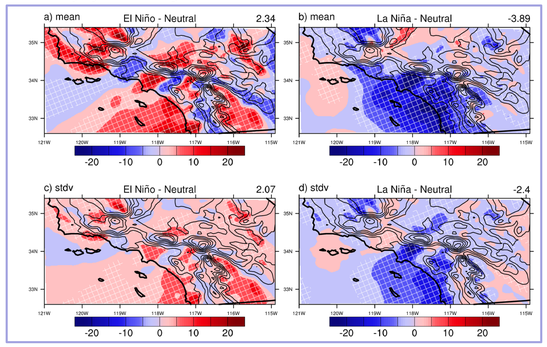

Fig. 6: *Average percentage differences of the mean and standard deviation (stdv) for daily-mean wind power (for a hub height of 80 m) between El Niño (a,c) and La Niña (b,d) winters compared to neutral winters. Positive differences are shaded red and negative differences are shaded blue. Regions with significant differences (at the 90% level using the t-test) are hatched. The domain-averaged value is reported on the top right of each plot. Note differences between this figure and Fig. 3, indicating that the impacts between near-surface wind speeds and wind power are non-linear for some regions. This is likely due to the non-linear nature of the turbine power curve.*

Conclusions

A high-resolution long-term regional climate simulation over Southern California has allowed an analysis of ENSO impacts on near-surface circulations. The strongest signals are general increases of average wind speeds and wind speed variability during El Niño (Fig. 2). More than half of the Southern California region experiences increased mean wind speeds during El Niño, while nearly 80% of the region experiences increased wind speed variability (Fig. 3a,c). Opposite, and nearly as strong, signals are also seen during La Niña. A majority of the Southern California region experiences decreased wind speed variability during La Niña events. Similarly, more than half of the region experiences reduced average wind speeds during La Niña, though this signal is not seen in the regionally-averaged time series of mean winter wind speeds (Figs. 2, 3b,d).

A cluster analysis technique was used to explain that shifts in prominent wintertime wind regimes are responsible for the significant spatial structures of the ENSO impacts (Figs. 3-5, Table 2). Generally, the onshore regime occurs more frequently during El Niño and occurs less frequently during La Niña. Meanwhile, the Santa Ana regime occurs less frequently during El Niño.

Near-surface circulation impacts are translated into wind power impacts and highlighted through a hypothetical wind farm off the coast of Los Angeles. It is found that ENSO impacts average wind power on the order of 10%, while the variability of wind power is impacted by approximately 5% at the wind farm (Fig. 6).

The results of this study agree with near-surface wind field impacts predicted through ENSO teleconnection dynamics. Frequent incursions of a stronger and southward displaced jet stream during El Niño leads to increased onshore events, bringing greater average speeds and wind speed variability over a large portion of Southern California. Conversely, a less direct and northward displaced jet stream during La Niña leads to a reduction of onshore events, and lower mean speeds and wind speed variability over much of Southern California.